Micron 68 (2014) 152–157

Contents lists available at ScienceDirect

Micron

journal homepage: www.elsevier.com/locate/micron

Electron-induced Ti-rich surface segregation on $SrTiO_3$ nanoparticles

Yuyuan Lin[a,*], Jianguo Wen[b], Linhua Hu[c], James A. McCarthy[c], Shichao Wang[c], Kenneth R. Poeppelmeier[c], Laurence D. Marks[a,*]

[a] Department of Materials Science and Engineering, Northwestern University, Evanston, IL 60208, United States
[b] Electron Microscopy Center, Argonne National Laboratory, Argonne, IL 60439, United States
[c] Department of Chemistry, Northwestern University, Evanston, IL 60208, United States

ARTICLE INFO

Article history:
Available online 2 June 2014

Keywords:
Beam damage
HREM
Surface structure
Simulation
Strontium titanate
Nanoparticles

ABSTRACT

Atomic surface structures of nanoparticles are of interest in catalysis and other fields. Aberration-corrected HREM facilitates direct imaging of the surfaces of nanoparticles. A remaining concern of surface imaging arises from beam damage. It is important to identify the intrinsic surface structures and the ones created by electron beam irradiation in TEM. In this study, we performed aberration-corrected HREM and EELS to demonstrate that TiO and bcc type Ti islands form due to intense electron irradiation. The formation of Ti-rich islands is in agreement with previous high temperature annealing experiments on the surfaces of $SrTiO_3$ single crystals.

High resolution electron microscopy (HREM) profile-view surface imaging is particularly useful for studying the surface structures of nanoparticles (Marks and Smith, 1983). Imaging the atomic surface structures of nanoparticles can bridge the so-called "materials gap" problem in surface science studies. The materials gap usually refers to the research emphasis on single crystal surfaces while the potential applications for catalysis are the surfaces of catalyst nanoparticles. Conventional HREM imaging with highly coherent FEG sources suffers from the image delocalization problems due to the large values of delocalization ($\nabla\chi$) and envelope terms beyond the first zero of the contrast-transfer function. Therefore it requires extensive HREM simulations to understand the experimental contrast. We note that this was not an issue with the original work (Marks, 1984, 1985) since less coherent LaB_6 sources were used – FEG sources make HREM harder to interpret. With the implementation of aberration correctors (Haider et al., 1998), the image delocalization in FEG instruments is significantly reduced and the surface atoms can be clearly visualized. Recently the surfaces of Co_3O_4 (Yu et al., 2010), $SrTiO_3$ (Lin et al., 2013), CeO_2 (Lin et al., 2014) nanoparticles were solved at atomic resolution by using aberration-corrected HREM. Usually the high electron dose in aberration-corrected HREM studies results in a high signal-to-noise ratio in the images. However the high electron dose can also induce significant damage to intrinsic surface structures. In this report, we demonstrate the formation of TiO and bcc type Ti islands on $SrTiO_3$ nanocuboids due to electron beam irradiation.

The surface structures of $SrTiO_3$ single crystals are well-studied, particularly for the (0 0 1) surface. $SrTiO_3$ has a perovskite structure, which is composed of a sequential stacking of SrO and TiO_2 layers along the [0 0 1] direction. Depending upon prior treatments, for instance ion-beam cleaning and chemical etching/exposure, point defects can diffuse from the bulk to the surface sink, the surface can be simple or complicated. Despite many years of work the exact details of what matters is still unclear, and sometimes the surfaces are "graduate student dependent", that is a given recipe can give different results. A variety of surface reconstructions have been observed after annealing ion-beam thinned/cleaned $SrTiO_3$ single crystals at high temperatures (Erdman et al., 2002, 2003; Herger et al., 2007; Kienzle et al., 2011; Lin et al., 2011; Newell, 2007). The solved surface reconstructions are TiO_2-rich, for reasons which are still not fully understood. In addition to the flat surface reconstructions, step-terrace structures (Baniecki et al., 2008; Sum et al., 1994), ridges (Sheiko et al., 1993), canyon-like features (Szot and Speier, 1999), and islands (Lee et al., 2005) on $SrTiO_3$ (0 0 1) surfaces have been revealed by microscopic techniques. In some cases the SrO-rich Ruddlesden–Popper (RP) phase forms on the $SrTiO_3$ surface above 900 °C (Szot et al., 1996), or prolonged annealing and higher temperatures can result in droplet-like features which were attributed to SrO (Szot and Speier, 1999). The droplet-like features can further agglomerate to form regular microcrystals on the surface. In contrast, TiO_2-rich surfaces with TiO or Ti_2O phases were observed on the $SrTiO_3$ surface under strongly reducing annealing environment above 900 °C, depending on the extent of reduction

* Corresponding authors. Tel.: +1 847 491 3996; fax: +1 847 491 7820.
E-mail addresses: YuyuanLin2014@u.northwestern.edu (Y. Lin), L-marks@northwestern.edu (L.D. Marks).

http://dx.doi.org/10.1016/j.micron.2014.05.007
0968-4328/

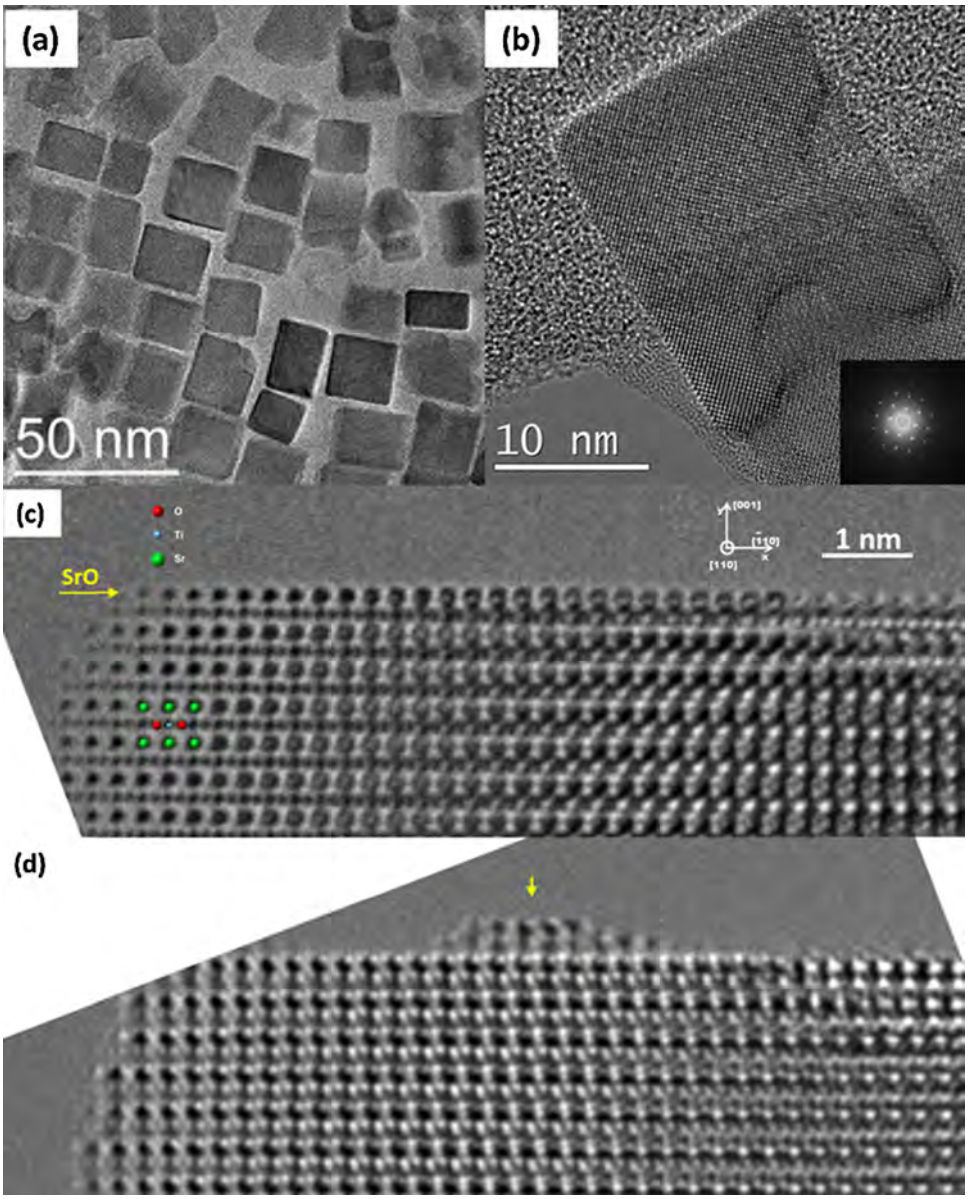

Fig. 1. (single-column) Shapes and surfaces of $SrTiO_3$ nanocuboids. (a) A low magnification image shows the general shapes of $SrTiO_3$ nanocuboids. (b) A HREM image of a $SrTiO_3$ nanocuboid in [1 0 0] zone axis. (c) A HREM image in [1 1 0] zone axis showing a flat (0 0 1) surface was observed initially, and was assigned to be the intrinsic surface. (d) With a ~2 nm converged electron probe applied on the nanocuboids for ~5 s, an additional island can be observed clearly, as indicated by the yellow arrow. (For interpretation of the references to color in this figure legend, the reader is referred to the web version of the article.)

(Szot and Speier, 1999). Similar results were observed on the surfaces of (La, Nb, Fe) doped $SrTiO_3$ crystals (Gunhold et al., 2003; Szot et al., 2000) as well as other perovskite materials such as $SrLaAlO_4$ (Becerra-Toledo and Marks, 2010). Rühle et al. observed TiO islands formed on the $SrTiO_3$ (0 0 1) surface with in situ HREM after annealing at 970 °C (Lee et al., 2005). In the present work, we show that in the high vacuum TEM column, nanoscale TiO and bcc type Ti islands form with intense electron beam irradiation.

1. Experiment

$SrTiO_3$ nanocuboids were synthesized via a hydrothermal method with oleic acid as a capping material (Hu et al., 2013). The as-prepared nanocuboids were collected and dried at 90 °C for ~12 h. The dry nanocuboids were dispersed in ethanol and deposited on a Cu TEM grid. The grid was then transferred into a FEI-titan 80–300 TEM with Cc and Cs aberration correctors installed, operating at 200 KeV. The base pressure of the specimen column was $\sim 1 \times 10^{-7}$ Torr. All the aberrations up to C_5 were tuned to an acceptable level (Cc < 1 μm, Cs = ~0 μm, astigmatisms and coma ~0 μm, $C_5 \sim -1$ mm) before recording the HREM images. After the nanocuboids were tilted to the [1 0 0] or [1 1 0] zone axis, time-series or focal-series images were taken with an exposure time of 1 s for each image. The electron dose was measured as $\sim 4 \times 10^6$ e/nm^{2}s for imaging. However, if the beam is focused to a small area (~2 nm in diameter) on the nanocuboids, severe specimen damage can be observed. For the latter case the dose can be two orders larger than the imaging mode. HREM simulation was performed using the MactempasX program based on multislice method (Cowley and Moodie, 1957) and conventional non-linear imaging theory (O'Keefe, 1979). The simulation parameters for simulated images are listed in the figure captions. The EELS measurement was conducted in TEM diffraction mode. The beam was converged to a ~2 nm diameter area to enhance the spatial resolution.

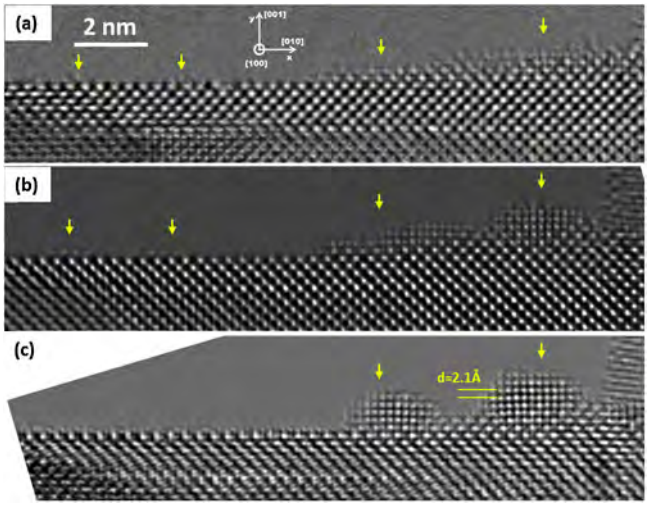

Fig. 2. (2-column) Evolution of the $SrTiO_3$ (0 0 1) surface under electron beam irradiation. (a), (b) and (c) were obtained by focusing the beam on the nanocuboids for ~3 s, 6 s, and 9 s, respectively. In (a), beam induced additional layers start to form. In (c), TiO islands formed. The lattice spacing is 2.1 Å, as indicated by the yellow lines. (For interpretation of the references to color in this figure legend, the reader is referred to the web version of the article.)

2. Result and discussion

The average size of $SrTiO_3$ nanocuboids is ~20 nm, as shown in Fig. 1(a) and (b). When the nanocuboids are tilted to the [1 0 0] or [1 1 0] zone axis, the mainly exposed {0 0 1} facets can be clearly imaged, as shown in Fig. 1(b) and (c) respectively. The intrinsic exposed (0 0 1) surface should be generally flat, as shown in Fig. 1(c). Due to the cuboid shape, the thickness is increasing from left to right in Fig. 1(c). At the thin region with slight underfocus imaging condition, the atoms appear as black spots. As the thickness increases, the intensity of the spots is oscillating due to the electron channeling in atom columns. Nevertheless, the surface is atomically flat and a SrO termination is present as the undamaged intrinsic surface structure, which is in agreement with our previous observation (Lin et al., 2013). However, if an intense beam is focused on the specimen for a few seconds, additional surface layers stack up on the original flat surface. Fig. 1(d) was obtained by focusing the electron beam on the specimen for ~5 s.

The results are reproducible. Fig. 2 shows the surface evolution under electron beam irradiation on a nanocuboid tilted to the [1 0 0] zone axis. Fig. 2(a), (b) and (c) were obtained by focusing the beam on the nanocuboids for ~3 s, 6 s, and 9 s, respectively. The HREM images show a square lattice with a lattice spacing of ~2.1 Å on the islands. The spacing is ~8% larger than the spacing of the (2 0 0) planes of $SrTiO_3$. After searching for possible crystal structures in Ti oxides, Sr oxides, and RP phases, only TiO with a lattice parameter of ~4.15 Å is close to the experimental measurement. Both TiO and SrO have a rocksalt structure, and therefore the square lattice should be present in the [1 0 0] viewing direction. However, the SrO crystal has a lattice parameter of ~5.1 Å, which is substantially different from the experiment. Fig. 3(b) and (c) shows atomic resolution experimental and simulated HREM images of a TiO island on $SrTiO_3$ surface. In Fig. 3, the black spots are atoms, as the image was taken at underfocus condition. The simulated image matches well with the experimental image, which further confirms the TiO phase of the islands. In addition, we conducted EELS measurements on the surface islands and on the nanocuboids successively, as shown in Fig. 4. The EELS results show the islands have a significant Sr deficiency compared to the bulk region. The absolute counts of the Ti L-edge on the islands are less than the bulk region due to the thickness difference. However, the quantification shows a substantial increase of Ti/O ratio on the islands compared to the bulk region.

The results in this study are similar to previous results of high temperature treatment of $SrTiO_3$ under reducing conditions, as well as electron-beam radiolytic damage studies of other oxides (e.g. (Ai et al., 1993; Fan and Marks, 1989; McCartney et al., 1991; Petford et al., 1986; Strane et al., 1988; Zhang and Marks, 1989)). The electron beam irradiation as well as the high vacuum almost certainly created a reducing environment on $SrTiO_3$ nanocuboids. However, the TiO island formation is not caused by electron-induced heating. The estimated temperature increase based on the inelastic scattering model is only a few degrees (Egerton et al., 2004). The dominant process is radiolytic damage for which the simplest model is the Knotek–Feibelman mechanism (Feibelman and Knotek, 1978; Knotek and Feibelman, 1978, 1979). The irradiating electron beam excites the core-level electron of the metal, which is followed by emission of Auger electrons from oxygen atoms. The resulting O atom is neutral or positively charged, and can be ejected to vacuum rather easily.

The mechanism of the formation of Ti-rich surface segregation in the present $SrTiO_3$ case is more complex than for binary compounds. In defect chemistry (Menesklou et al., 1999; Moos and Hardtl, 1997), it is believed the predominant ionic point defects are Sr and O vacancies (V''_{Sr} and $V^{\cdot\cdot}_{O}$). The surface segregation can be possibly assigned to V''_{Sr} and $V^{\cdot\cdot}_{O}$ vacancies. There is a Coulombic attraction between V''_{Sr} and $V^{\cdot\cdot}_{O}$, as V''_{Sr} and $V^{\cdot\cdot}_{O}$ are negatively and positively charged (Lee et al., 2013). A large amount of $V^{\cdot\cdot}_{O}$ are created at the surface region by the electron beam, which can cause the enrichment in V''_{Sr} and $V^{\cdot\cdot}_{O}$ at the surface. The V''_{Sr} and $V^{\cdot\cdot}_{O}$ enrichment leads to a Ti-rich $SrTiO_3$ surface. The equilibrium concentration of thermally-activated point defects of $SrTiO_3$ at room temperature is exceedingly low (Meyer et al., 2003). The formation and diffusion of vacancies in this case can be attributed to the electron beam (Singh and Marks, 1989).

A remaining question is why the TiO islands are grown instead of double-layered TiO_2-rich surface reconstructions (Erdman et al., 2002). In this study, it seems that additional surface layers are present locally at the early stages of electron beam irradiation on the surface, as indicated by the arrows in Fig. 2(a) and (b). At later stages, the atoms at the additional surface layers seem to agglomerate and form islands. According to the phase diagram predicted by a DFT study (Heifets et al., 2007), it is energetically preferable to form Ti-rich precipitates at low O pressure and high temperature. In the region where the bulk $SrTiO_3$ is not stable, the energy required to form Ti-rich islands or microcrystals is lower than that for the formation of the layer-by-layer TiO_2-rich surface. A more recent study pointed out that it is important to relate sample preparation history to the stability of different surface structures of $SrTiO_3$ (Marks et al., 2009). The present work demonstrates that for the non-stoichiometric nanocuboids (SrO-terminated surfaces), TiO islands are at least stable under intense electron beam irradiation in high vacuum.

The majority of the surface islands are TiO, as shown in Fig. 5(a). We also observed a small portion of Ti islands. Fig. 5(b) shows a HREM image of a different type of island on $SrTiO_3$ nanocuboids. The lattice spacing is ~3.3 Å, smaller than the ~4.15 Å for the lattice parameter of TiO. In addition to the different lattice spacing, the lattice pattern differs from the fcc lattice of the rocksalt TiO. We found the oxides of Ti and Sr do not have lattice parameters and lattice patterns similar to the experiment. Only the bcc type Ti metal (space group Im-3 m) can have such lattice pattern and lattice parameters. A set of simulated HREM images with varying thickness and defocus using the TiO and bcc type Ti (bcc-Ti) structures is shown in Fig. 5(c) and (d). The simulated images of TiO always show a square-on-square lattice pattern while the

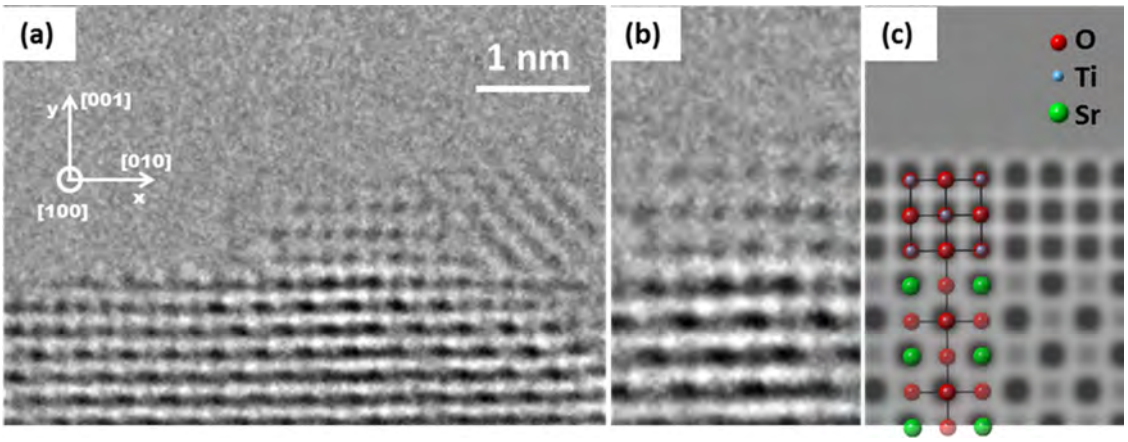

Fig. 3. (1.5-column) Atomic resolution HREM images showing the interfacial structure of TiO and SrO-terminated $SrTiO_3$. (a) Experimental HREM image taken at a small underfocus condition. (b) Cropped and magnified images of (a). (c) Simulated HREM image for (b). The simulation parameters are thickness = 3 nm, defocus = −2 nm, Cs = −5 μm, convergence angle = 0.3 mrad, focal spread = 3.5 nm, vibration = 0.4 Å in both *x* and *y* directions. No astigmatisms, coma, and sample tilt were considered in the simulation. The lattice spacing for $SrTiO_3$ and TiO are all set to 4.1 Å, thus no lattice strain can be seen in the simulation.

simulated images of bcc-Ti show a checkerboard lattice pattern, which matches with the experiment. By investigating the phase diagram of Ti–O binary systems, the bcc phase can be a solid solution of O in Ti matrix. Thus strictly speaking the bcc-Ti is bcc-TiO_x (x up to ~0.08) (Cancarevic et al., 2007). The presence of TiO_x islands may arise from further reduction of the TiO islands.

It is worth noting that $SrTiO_3$ is a relatively robust material under electron irradiation for most TEM studies (Erdman et al., 2002; Zhu et al., 2012). In this study, however, a high flux was used with the beam converged to a small probe. The Ti-rich surface segregation is very similar to that observed previously on $SrTiO_3$ single crystals after hours of high temperature annealing, which were attributed to the point defect chemistry of $SrTiO_3$. It has been demonstrated that Ti-rich surface segregation occurred after the amorphous carbon film on the surface was removed (Lee et al., 2005). Our previous studies have shown that the encapsulating carbon layer on the surface can reduce the beam damage (Strane et al., 1988), as the loss of oxygen is much slower with the contamination layer present. $SrTiO_3$ nanocuboids with clean surfaces are thus more vulnerable to beam damage. It should be noted that this surface segregation is not the only damage that an intense electron beam can induce. We have observed other types of damages on $SrTiO_3$ such as hole-drilling with a converged electron probe. The different types of damage and their mechanisms have been studied previously (Egerton et al., 2004; Strane et al., 1988).

This study reveals that beam damage should be avoided in order to study intrinsic surface structures. In practice, whether or not the surfaces are still intrinsic in HREM images can be determined by surface roughness in the case of $SrTiO_3$. For some other reducible oxides, such as WO_3 (Petford et al., 1986) and $Ti_2Nb_{10}O_{29}$ (Smith and Bursill, 1985), prolonged exposure to the electron beam show several metallic layers at the surface region. Therefore, a phase diagram of surface damage for specific materials with respect to total electron dose can be created. The investigation of intrinsic surface

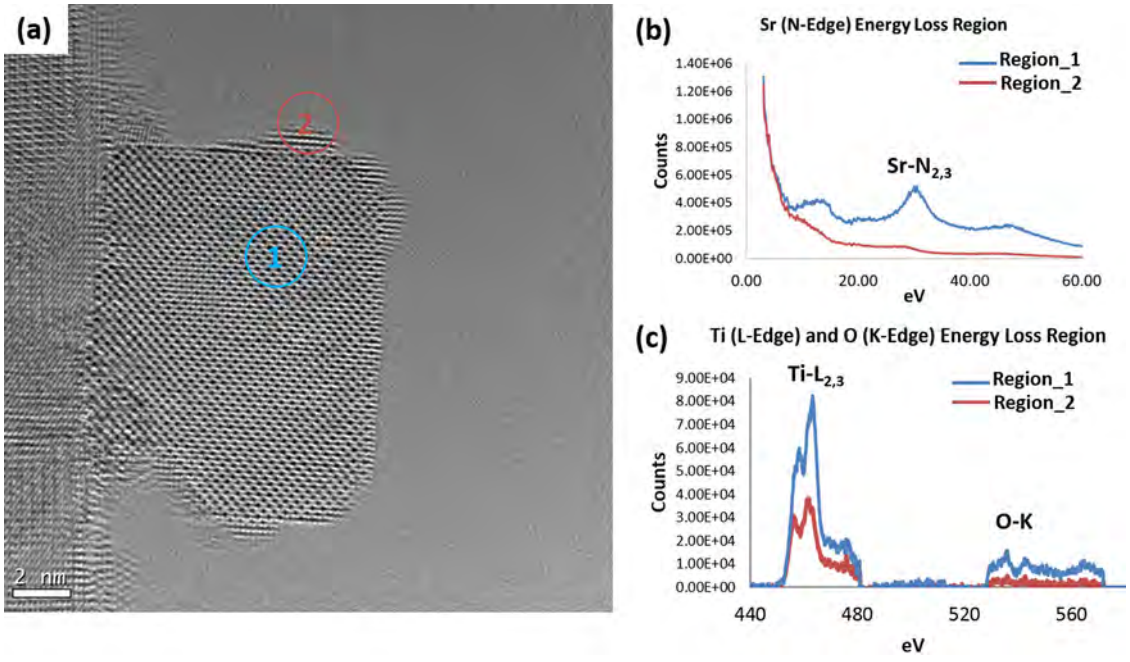

Fig. 4. (2-column) (a) Illustration of the regions conducted EELS measurements. (b) and (c) EELS results showing the difference of Sr N-edge, Ti L-edge, and O K-edge of the two regions as indicated in (a).

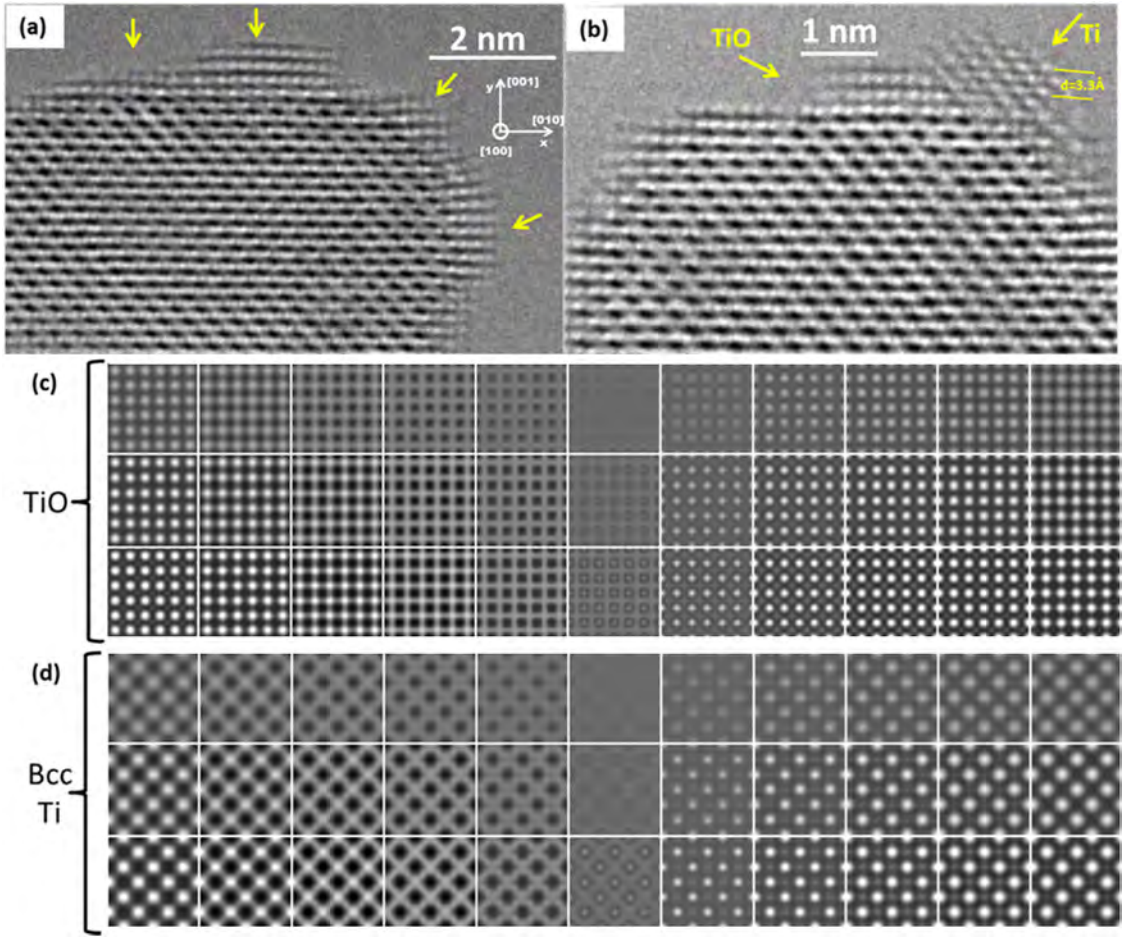

Fig. 5. (2-column) Comparison between TiO and Ti islands. (a) Experimental image showing TiO islands on the $SrTiO_3$ surfaces. (b) shows a Ti island beside a TiO island. (c) Series of simulated HREM images with thickness changes vertically from 1 nm on top to 3 nm on the bottom and defocus changes horizontally from −10 nm on the left to 10 nm on the right. Each image represents a 3×3 cell in the [1 0 0] zone axis. (d) The simulated HREM images with the same setting of (c) except using a bcc-Ti model. The simulation parameters other than the thickness and defocus are the same as the ones used in Fig. 3.

structures by HREM should be done with an electron dose less than the threshold to cause damage. Recently, this approach has been used by Yoshida et al. using environmental TEM to differentiate intrinsic and electron induced shapes of supported Au nanoparticles (Kuwauchi et al., 2012). If the beam damage effect is not carefully calibrated, other characterization techniques should be used to confirm the findings of HREM profile-surface imaging.

3. Conclusions

In summary, we demonstrate that TiO and Ti islands form on the (0 0 1) surface of $SrTiO_3$ nanocuboids due to intense electron beam irradiation. The results are similar to previous studies on $SrTiO_3$ single crystals using high temperature annealing under reducing conditions, and may be extended to the surfaces of other perovskite materials.

Acknowledgements

We acknowledge funding from the Northwestern University Institute for Catalysis in Energy Processes (ICEP) on grant number DOE DE-FG02-03-ER15457. The electron microscopy was performed at the Electron Microscopy Center for Materials Research at Argonne National Laboratory, a U.S. Department of Energy Office of Science Laboratory operated under Contract No. DE-AC02-06CH11357 by UChicago Argonne, LLC.

References

Ai, R., Fan, H.J., Marks, L.D., 1993. Phase transition kinetics in DIET of vanadium pentoxide: I. Experimental results. Surf. Sci. 280, 369–374.
Baniecki, J.D., Ishii, M., Kurihara, K., Yamanaka, K., Yano, T., Shinozaki, K., Imada, T., Nozaki, K., Kin, N., 2008. Photoemission and quantum chemical study of $SrTiO_3$(0 0 1) surfaces and their interaction with CO_2. Phys. Rev. B 78, 195415.
Becerra-Toledo, A.E., Marks, L.D., 2010. Strontium oxide segregation at $SrLaAlO_4$ surfaces. Surf. Sci. 604, 1476–1480.
Cancarevic, M., Zinkevich, M., Aldinger, F., 2007. Thermodynamic description of the Ti–O system using the associate model for the liquid phase. CALPHAD 31, 330–342.
Cowley, J.M., Moodie, A.F., 1957. The scattering of electrons by atoms and crystals. 1. A new theoretical approach. Acta Crystallogr. 10, 609–619.
Egerton, R.F., Li, P., Malac, M., 2004. Radiation damage in the TEM and SEM. Micron 35, 399–409.
Erdman, N., Poeppelmeier, K.R., Asta, M., Warschkow, O., Ellis, D.E., Marks, L.D., 2002. The structure and chemistry of the TiO_2-rich surface of $SrTiO_3$(0 0 1). Nature 419, 55–58.
Erdman, N., Warschkow, O., Asta, M., Poeppelmeier, K.R., Ellis, D.E., Marks, L.D., 2003. Surface structures of $SrTiO_3$ (0 0 1): a TiO_2-rich reconstruction with a c(4 × 2) unit cell. J. Am. Chem. Soc. 125, 10050–10056.
Fan, H.J., Marks, L.D., 1989. Phase transitions in V_2O_5 in a high resolution electron microscope. Ultramicroscopy 31, 357–364.
Feibelman, P.J., Knotek, M.L., 1978. Reinterpretation of electron-stimulated desorption data from chemisorption systems. Phys. Rev. B 18, 6531–6539.
Gunhold, A., Beuermann, L., Frerichs, M., Kempter, V., Gömann, K., Borchardt, G., Maus-Friedrichs, W., 2003. Island formation on 0.1 at.% La-doped $SrTiO_3$(1 0 0) at elevated temperatures under reducing conditions. Surf. Sci. 523, 80–88.
Haider, M., Uhlemann, S., Schwan, E., Rose, H., Kabius, B., Urban, K., 1998. Electron microscopy image enhanced. Nature 392, 768–769.
Heifets, E., Piskunov, S., Kotomin, E.A., Zhukovskii, Y.F., Ellis, D.E., 2007. Electronic structure and thermodynamic stability of double-layered $SrTiO_3$ (0 0 1) surfaces: ab initio simulations. Phys. Rev. B 75, 115417.

Herger, R., Willmott, P.R., Bunk, O., Schleputz, C.M., Patterson, B.D., Delley, B., 2007. Surface of strontium titanate. Phys. Rev. Lett. 98, 076102.
Hu, L., Wang, C., Lee, S., Winans, R.E., Marks, L.D., Poeppelmeier, K.R., 2013. $SrTiO_3$ nanocuboids from a lamellar microemulsion. Chem. Mater. 25, 378–384.
Kienzle, D.M., Becerra-Toledo, A.E., Marks, L.D., 2011. Vacant-site octahedral tilings on $SrTiO_3$(0 0 1), the ($\sqrt{13} \times \sqrt{13}$)R33.7° surface, and related structures. Phys. Rev. Lett. 106, 176102.
Knotek, M.L., Feibelman, P.J., 1978. Ion desorption by Core–Hole Auger decay. Phys. Rev. Lett. 40, 964–967.
Knotek, M.L., Feibelman, P.J., 1979. Stability of ionically bonded surfaces in ionizing environments. Surf. Sci. 90, 78–90.
Kuwauchi, Y., Yoshida, H., Akita, T., Haruta, M., Takeda, S., 2012. Intrinsic catalytic structure of gold nanoparticles supported on TiO_2. Angew. Chem. Int. Ed. 51, 7729–7733.
Lee, S.B., Phillipp, F., Sigle, W., Rühle, M., 2005. Nanoscale TiO island formation on the $SrTiO_3$(0 0 1) surface studied by in situ high-resolution transmission electron microscopy. Ultramicroscopy 104, 30–38.
Lee, W., Han, J.W., Chen, Y., Cai, Z., Yildiz, B., 2013. Cation size mismatch and charge interactions drive dopant segregation at the surfaces of manganite perovskites. J. Am. Chem. Soc. 135, 7909–7925.
Lin, Y., Becerra-Toledo, A.E., Silly, F., Poeppelmeier, K.R., Castell, M.R., Marks, L.D., 2011. The (2 × 2) reconstructions on the $SrTiO_3$ (0 0 1) surface: a combined scanning tunneling microscopy and density functional theory study. Surf. Sci. 605, L51–L55.
Lin, Y., Wen, J., Hu, L., Kennedy, R.M., Stair, P.C., Poeppelmeier, K.R., Marks, L.D., 2013. Synthesis-dependent atomic surface structures of oxide nanoparticles. Phys. Rev. Lett. 111, 156101.
Lin, Y., Wu, Z., Wen, J., Poeppelmeier, K.R., Marks, L.D., 2014. Imaging the atomic surface structures of CeO_2 nanoparticles. Nano Lett. 14, 191–196.
Marks, L.D., 1984. Direct atomic imaging of solid-surfaces. 1. Image simulation and interpretation. Surf. Sci. 139, 281–298.
Marks, L.D., 1985. Image localization. Ultramicroscopy 18, 33–37.
Marks, L.D., Chiaramonti, A.N., Tran, F., Blaha, P., 2009. The small unit cell reconstructions of $SrTiO_3$(1 1 1). Surf. Sci. 603, 2179–2187.
Marks, L.D., Smith, D.J., 1983. Direct surface imaging in small metal particles. Nature 303, 316–317.
McCartney, M.R., Crozier, P.A., Weiss, J.K., Smith, D.J., 1991. Electron-beam-induced reactions at transition-metal oxide surfaces. Vacuum 42, 301–308.
Menesklou, W., Schreiner, H.-J., Härdtl, K.H., Ivers-Tiffée, E., 1999. High temperature oxygen sensors based on doped $SrTiO_3$. Sens. Actuators B: Chem. 59, 184–189.
Meyer, R., Waser, R., Helmbold, J., Borchardt, G., 2003. Observation of vacancy defect migration in the cation sublattice of complex oxides by ^{18}O tracer experiments. Phys. Rev. Lett. 90, 105901.
Moos, R., Hardtl, K.H., 1997. Defect chemistry of donor-doped and undoped strontium titanate ceramics between 1000° and 1400 °C. J. Am. Ceram. Soc. 80, 2549–2562.
Newell, D.T., 2007. University of Cambridge (Ph.D. thesis).
O'Keefe, M.A., 1979. Resolution-damping functions in non-linear images. In: Proceedings of the 37th annual electron microscopy society of America meeting, Claitor's, San Antonio, TX, p. 556.
Petford, A.K., Marks, L.D., O'Keeffe, M., 1986. Atomic imaging of oxygen desorption from tungsten trioxide. Surf. Sci. 172, 496–508.
Sheiko, S.S., Möller, M., Reuvekamp, E.M.C.M., Zandbergen, H.W., 1993. Calibration and evaluation of scanning-force-microscopy probes. Phys. Rev. B 48, 5675–5678.
Singh, S.R., Marks, L.D., 1989. Diffusion during electron-beam-induced reduction of tungsten trioxide. Philos. Mag. Lett. 60, 31–36.
Smith, D.J., Bursill, L.A., 1985. Metallisation of oxide surfaces observed by in situ high-resolution electron microscopy. Ultramicroscopy 17, 387–391.
Strane, J., Marks, L.D., Luzzi, D.E., Buckett, M.I., Zhang, J.P., Wessels, B.W., 1988. Encapsulation, diffusion and diet in the electron microscope. Ultramicroscopy 25, 253–257.
Sum, R., Lüthi, R., Lang, H.P., Güntherodt, H.J., 1994. Scanning force microscopy on polished single crystalline $SrTiO_3$(1 0 0) substrates used for high Tc superconductor thin film deposition. Phys. C: Superconduct. 235–240, 621–622, Part 1.
Szot, K., Speier, W., 1999. Surfaces of reduced and oxidized $SrTiO_3$ from atomic force microscopy. Phys. Rev. B 60, 5909–5926.
Szot, K., Speier, W., Breuer, U., Meyer, R., Szade, J., Waser, R., 2000. Formation of micro-crystals on the (1 0 0) surface of $SrTiO_3$ at elevated temperatures. Surf. Sci. 460, 112–128.
Szot, K., Speier, W., Herion, J., Freiburg, C., 1996. Restructuring of the surface region in $SrTiO_3$. Appl. Phys. A 64, 55–59.
Yu, R., Hu, L.H., Cheng, Z.Y., Li, Y.D., Ye, H.Q., Zhu, J., 2010. Direct subangstrom measurement of surfaces of oxide particles. Phys. Rev. Lett. 105, 226101.
Zhang, J.P., Marks, L.D., 1989. Symmetry in DIET phase transitions. Surf. Sci. 222, 13–20.
Zhu, G.-z., Radtke, G., Botton, G.A., 2012. Bonding and structure of a reconstructed (0 0 1) surface of $SrTiO_3$ from TEM. Nature 490, 384–387.